The Astrophysical Journal, 644:274–278, 2006 June 10

X-RAY OBSERVATIONS OF SN 1006 WITH *INTEGRAL*

E. Kalemci,[1,2] S. P. Reynolds,[3] S. E. Boggs,[1,4] N. Lund,[5] J. Chenevez,[5] M. Renaud,[6,7] and J. Rho[8]

Received 2005 July 26; accepted 2006 February 14

ABSTRACT

The remnant of the supernova of 1006 AD, the remnant first showing evidence for the presence of X-ray synchrotron emission from shock-accelerated electrons, was observed for ~1000 ks with *INTEGRAL* in order to study electron acceleration to very high energies. The aim of the observation was to characterize the synchrotron emission and attempt to detect nonthermal bremsstrahlung using the combination of IBIS and JEM-X spatial and spectral coverage. The source was detected with JEM-X between the 2.4 and 8.4 keV bands and was not detected with either ISGRI or SPI above 20 keV. The ISGRI upper limit is about a factor of 4 above current model predictions, but confirms the presence of steepening in the power law extrapolated from lower energies (<4 keV).

Subject headings: ISM: individual (SN 1006) — radiation mechanisms: nonthermal — supernova remnants — X-rays: ISM

Online material: color figures

1. INTRODUCTION

Supernova remnants (SNRs) have long been thought to be the primary site of Galactic cosmic ray acceleration up to the "knee" feature in the integrated cosmic-ray spectrum near 3000 TeV, as the supernova shocks are one of the few mechanisms that could provide enough energy to support this population (Dyer et al. 2001). However, many features of the acceleration process, including injection physics, efficiency, and maximum electron and ion energies, are not yet clear. Hard X-ray observations (above 10 keV) of SNRs may cast light on this poorly understood process.

High-energy electrons in SNRs produce X-rays via two mechanisms, nonthermal bremsstrahlung and synchrotron radiation. Electrons can also produce gamma-rays up to TeV energies by inverse Compton (IC) scattering of any photons present, such as the cosmic microwave background (CMB). In addition, relativistic protons can produce gamma-rays from the decay of π^0 particles from inelastic ion-ion collisions. All these processes have been extensively modeled for SNRs by various groups (Sturner et al. 1997; Gaisser et al. 1998; Baring et al. 1999). In hard X-rays, synchrotron radiation from the tail of the electron distribution may compete with nonthermal bremsstrahlung from the very lowest energy accelerated electrons.

SN 1006 has been the prototype laboratory for the study of electron acceleration to high energies in shocks. X-rays from this object were first reported by Winkler & Laird (1976). The earlier featureless spectrum (Becker et al. 1980) was modeled as the loss-steepened extrapolation of the radio synchrotron spectrum by Reynolds & Chevalier (1981). Later, observations by *ASCA* (Koyama et al. 1995) showed that the limbs have featureless spectra well described by power laws, whereas the interior has a thermal, line-dominated spectrum. The source was also observed with the *Rossi X-Ray Timing Explorer* (*RXTE*), and Dyer et al. (2001) showed that elaborate synchrotron emission models (Reynolds 1996, 1998) fit the combined *RXTE*+*ASCA* spectrum reasonably well.

Electrons producing keV synchrotron emission could also produce very high energy photons (in the TeV range) by IC upscattering of CMB photons (Pohl 1996). The TeV flux depends on the electron distribution, and in conjunction with the synchrotron flux, a mean magnetic field strength of the remnant can be deduced. A detection of the northeast (NE) limb of SN 1006 was reported in ground-based TeV observations by CANGAROO-I (Tanimori et al. 1998). It is interesting that only one limb was detected, even though the X-ray spectra of the two limbs are similar (Allen et al. 2001; Dyer et al. 2004). To have a discrepancy in the TeV band, the electron spectra, magnetic field strengths, or synchrotron and IC emission angle distributions of the two rims would have to be different (Allen et al. 2001), but in a way that does not produce significant differences in the X-ray band.

The nature of X-ray emission from SN 1006 above 10 keV is still uncertain. Below 10 keV, synchrotron emission is the most plausible explanation. For synchrotron radiation, the quantitative inferences apply only to the exponential cutoff of the electron distribution. On the other hand, most of the accelerated electrons and much of their total energy reside in the lowest energy nonthermal electrons, whose bremsstrahlung emission could become dominant above 30 keV. In principle, the *International Gamma-Ray Astrophysics Laboratory* (*INTEGRAL*) can examine the effects of both the lowest and highest energy nonthermal electrons by distinguishing the synchrotron and bremsstrahlung emission with its imaging and spectral capabilities.

Reynolds (1999) modeled bremsstrahlung and synchrotron emission from SN 1006. Synchrotron hard X-rays should be concentrated in two bright opposing limbs, like the radio emission, and should dominate the emission below 30 keV. The images and spectra taken with *ASCA* (Koyama et al. 1995), *Chandra X-Ray Observatory* (Long et al. 2003), and *XMM-Newton* (Rothenflug et al. 2004) confirm this below 10 keV. The nonthermal bremsstrahlung, resulting from slightly suprathermal shock-accelerated

[1] Space Sciences Laboratory, 7 Gauss Way, University of California, Berkeley, CA 94720-7450.
[2] Sabancı University, Orhanlı-Tuzla 34956, İstanbul, Turkey.
[3] Department of Physics, North Carolina State University, 2700 Stinson Drive, Box 8202, Raleigh, NC 27695.
[4] Department of Physics, 366 Le Conte Hall, University of California, Berkeley, CA 94720-7300.
[5] Danish National Space Center, Juliane Maries Vej 30, DK-2100 Copenhagen Ø, Denmark.
[6] Service d'Astrophysique, CEA-Saclay, 91191, Gif-Sur-Yvette, France.
[7] APC-UMR 7164, 11 Place Marcelin Berthelot, 75231 Paris, France.
[8] *Spitzer* Science Center, California Institute of Technology, Mail Stop 220-6, Pasadena, CA 91125.

electrons interacting with thermal ions, is likely to be more symmetrically distributed, and will dominate at some energy between 30 and 300 keV. The bremsstrahlung flux will scale with the product of the thermal gas density nth and the relativistic electron density $n_{e,\mathrm{rel}}$. The former can be constrained by observations of thermal X-ray emission, while the latter can be deduced from radio synchrotron fluxes if the magnetic field is known.

The TeV spectrum reported from CANGAROO-I (Tanimori et al. 1998) could be well described by IC upscattered CMB photons, using a power-law electron spectrum with an exponential cutoff, as described in Dyer et al. (2001). This fit gave a postshock magnetic field of about 10 μG. However, this result is now called into question by the observations of the High-Energy Stereoscopic System (H.E.S.S.), which did not detect the source despite better sensitivity than CANGAROO-I. The TeV upper limits from H.E.S.S. are about a factor of 10 below the CANGAROO-I results[9] (Aharonian et al. 2005). These limits constrain IC upscattering of CMB photons by the same electrons that produce X-ray synchrotron emission; tighter limits mean fewer electrons, a higher magnetic field (Aharonian et al. [2005] place a lower limit of 25 μG on the postshock magnetic field), and less nonthermal bremsstrahlung. Lowering the possible IC-CMB flux by a factor of 10 directly lowers the allowable relativistic electron density by the same factor, and hence lowers the predicted bremsstrahlung flux by an order of magnitude.

Even if bremsstrahlung is not detected, the detailed shape of the steepening synchrotron spectrum can provide information on the physical process causing the cutoff in the electron spectrum. This is crucial information for understanding the acceleration of cosmic rays, since if the cutoff is due to radiative losses on electrons, the proton spectrum might extend to much higher energies, perhaps as high as the knee. However, if the finite remnant age (or size) or some change in diffusive properties of the upstream medium causes the cutoff, it should also cut the proton spectrum off at a similar energy (between 10 and 100 TeV; Dyer et al. 2001), far below the "knee" energy. Detailed models show subtle but potentially distinguishable differences in the shape of the synchrotron spectrum above 10 keV, with loss-limited spectra (due to higher magnetic fields) being somewhat harder.

Our group has observed SN 1006 for ~1000 ks with *INTEGRAL* (Winkler et al. 2003) in AO-1, with the main aim of detecting and characterizing synchrotron emission and distinguishing synchrotron and nonthermal bremsstrahlung emission by comparing the IBIS ISGRI and JEM-X images to the model images. In this work, we discuss the results of the analysis of the *INTEGRAL* data and place limits on the synchrotron and bremsstrahlung emission from SN 1006.

2. OBSERVATIONS AND ANALYSIS

The *INTEGRAL* observations took place in two sets. The ~250 ks first set ("set I") was conducted early in the mission, between 2003 January 11 and 20, corresponding to *INTEGRAL* revolutions 30 and 32. The ~750 ks second set ("set II") was conducted between 2004 January 20 and 30, during revolutions 155–158. These two sets have different observational characteristics for different instruments, as explained below, and only the data from set II are used for this paper. We did not use SPI (Spectrometer on *INTEGRAL*; Vedrenne et al. 2003), as ISGRI (see § 2.2 for more information) places much stricter limits in the hard X-ray band. Before the general analysis for all instruments, we filtered out the pointings with high anticoincidence shield rates, mostly occurring during the entry and exit of the radiation belts.

TABLE 1
JEM-X Summary

Energy Band (keV)	Flux (10^{-4} photons cm^{-2} s^{-1})	Statistical Significance	Model Flux[a] (10^{-4} photons cm^{-2} s^{-1})
NE Limb			
2.4–4.2[b]	10 ± 4	2.6	14
4.2–8.4	11 ± 2	5.0	5.9
8.4–14	3.3 ± 1.9	1.7	1.4
SW Limb			
2.4–4.2	15 ± 4	4.0	13
4.2–8.4	3.6 ± 2.3	1.6	4.8
8.4–14	<5.7	3[c]	...

[a] Flux from extrapolated model fit to the *ASCA* spectrum (0.8–9 keV; Dyer et al. 2004).
[b] The actual low energy threshold is variable over different parts of the JEM-X detector.
[c] 3 σ upper limit.

2.1. *The JEM-X Analysis*

The Joint European X-ray Monitor (JEM-X) consists of two identical high-pressure imaging microstrip gas chambers, and makes observations simultaneously with the main instruments on *INTEGRAL*, albeit with a narrower, fully coded field of view of 4°.8. The energy band is 3–35 keV, and the angular resolution is 3′.35 (Lund et al. 2003). Because a problem with eroding anodes, the high voltage in the JEM-X detectors was lowered, and a new background rejection criterion was implemented after the launch. One of the detector pair is being kept in a safe state, and during our observations only JEM-X 2 was operational.

Set I was conducted before the new background rejection criteria were implemented in JEM-X, and therefore was not included in this analysis. We note that although the total exposure for set II is ~750 ks, the effective exposure time of the central object is approximately 250 ks, due to the vignetting of the JEM-X instrument during the 25 point dither. We have obtained JEM-X images in 4 energy bands using the JEM-X Midisky offline software package available from the DNSC (Lund et al. 2004). These energy bands[10] are 2.4–4.2, 4.2–8.4, 8.4–14, and 14–35 keV. The images from each pointing are then mosaicked using the Mosaic Weight program (Chenevez et al. 2004).

The fluxes and the significance values shown in Table 1 are derived using the inner *ASCA* contours enclosing the NE and SW limbs to define two shape templates. The NE template is constructed with 23 pixels inside the inner *ASCA* contour seen as the upper left limb in Figure 1. The SW template is also constructed similarly, using the 19 pixels inside the lower right inner *ASCA* contour. The count excesses in the JEM-X mosaic images are then determined inside these two regions. The relevant noise figures are derived by defining a number of nonoverlapping regions with the reference templates within a 60×60 pixel field ($90'' \times 90''$) centered on SN 1006. 114 NE templates, each containing 23 pixels,

[9] Recent measurements by CANGAROO-III has also claimed null result on SN 1006 (Tanimori et al. 2005).

[10] The low energy threshold is variable over different parts of the JEM-X detector.

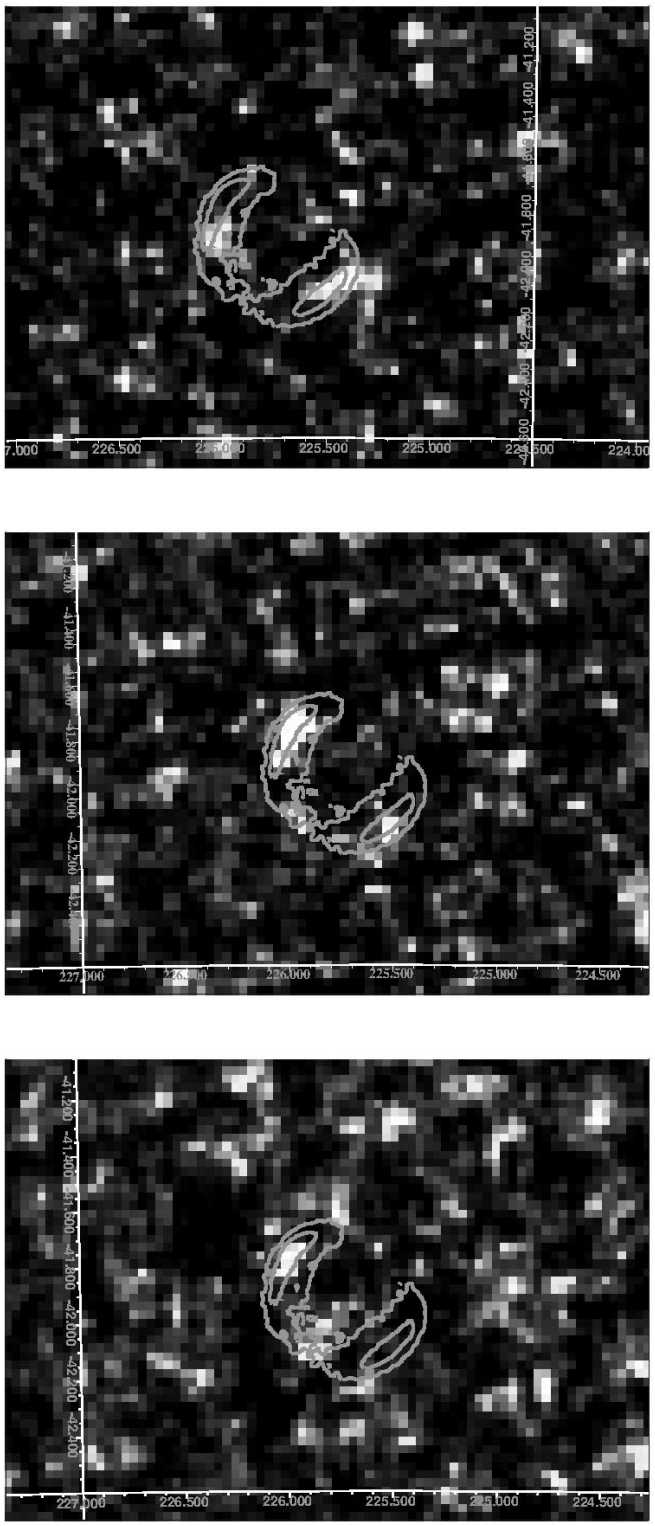

FIG. 1.—JEM-X reconstructed images of SN 1006 in three energy bands: 2.4–4.2 keV (*top*), 4.2–8.4 (*middle*) keV, and 8.4–14 keV (*bottom*). The *ASCA* contours are overlaid. The detection significances, fluxes, and upper limit fluxes are shown in Table 1. [*See the electronic edition of the Journal for a color version of this figure.*]

can be arranged within the 60×60 field. For the SW template the corresponding numbers are 112 regions, each with 19 pixels. The statistical properties of the excess counts in these two sets of regions are used to derive rms noise of the background for regions of the two shapes. The signal-to-noise ratio derived in this way will obey normal statistics, because the region templates are defined independently of the JEM-X data. The fluxes are derived by comparing the excesses in the SN 1006 mosaics with corresponding excesses in mosaic images of the Crab Nebula obtained with the same INTEGRAL dither pattern, and correcting for the difference in the effective observation time.

2.2. *The ISGRI Analysis*

One of the two main instruments on *INTEGRAL*, IBIS (Imager on Board the *INTEGRAL* Satellite; Ubertini et al. 2003), consists of two cameras. The *INTEGRAL* Soft Gamma-Ray Imager (ISGRI) is the low-energy camera of the IBIS telescope (Lebrun et al. 2003). It has a large sensitive area of 2621 cm^2 made up of 16,384 CdTe pixels. The angular resolution is $\sim 13'$ (Gros et al. 2003), and the fully coded field of view is 9°. The energy range is 20 keV to 10 MeV. The older background maps for set I observations resulted in much noisier images compared to set II images, and therefore we limit the analysis to the data from set II. We used OSA version 4.2 (Goldwurm et al. 2003) standard programs to obtain images in the 20–40 and 40–100 keV bands.

Since the ISGRI system point-spread function is $\sim 13'$, SN 1006 ($\sim 30'$ diameter) appears as an extended object to the imager. Estimation of the flux of such sources with a coded-mask instrument is complicated, since the mask patterns used in gamma-ray astronomy are optimized for point sources. One needs to use simulations to obtain the effect of the extended nature of the source on the image and the measured flux. Such simulations have been conducted for ISGRI for different extended source geometries, including SN 1006 (Renaud et al. 2006). For SN 1006 Renaud et al. (2006) used an input image of the expected synchrotron emission map in the 20–40 keV band based on the simulations described in Reynolds (1999). The principle of the ISGRI simulations is as follows. For each pointlike source constituting the extended one, the corresponding shadowgram (the image of the mask pattern illuminated and projected onto ISGRI) is calculated. The final expected shadowgram of SN 1006 is obtained by summing all these contributions. Then, the standard deconvolution (see Goldwurm et al. 2003 for details) in OSA is applied to obtain the reconstructed image. With this technique, Renaud et al. (2006) obtained a reduction factor of 0.7, i.e., ISGRI would detect 70% of the true flux at each limb.

3. RESULTS

3.1. *JEM-X Results*

The source is detected at the limbs in 2.4–4.2 and 4.2–8.4 keV bands (see Fig. 1 and Table 1). This is the first time that the structure of an individual extended source has been imaged with *INTEGRAL*. It appears that the SW limb (the limb on the right in the images) is stronger in the 2.4–4.2 keV band at about the 1 σ level, but the trend is reversed at higher energies. At 4.2–8.4 keV the NE limb is stronger, a result with higher significance. An excess at the position of the NE limb is present in the 8.4–14 keV band (1.7 σ), but no excess is seen in the SW limb. We note that the *XMM-Newton* data also point to an asymmetry in flux coming from the NE and SW limbs, such that the NE limb gets relatively stronger as energy increases (Rothenflug et al. 2004). A similar trend is seen in *ASCA* data (Dyer et al. 2004), but the differences are small in the *ASCA* band (below 8 keV). The small excess of the SW over NE limbs in the 2.4–4.2 keV band that we see is not supported by *ASCA* or *XMM-Newton* observations in that energy range.

Figure 2 shows our combined JEM-X fluxes for both limbs, compared with previous spatially integrated pre-*ASCA* flux

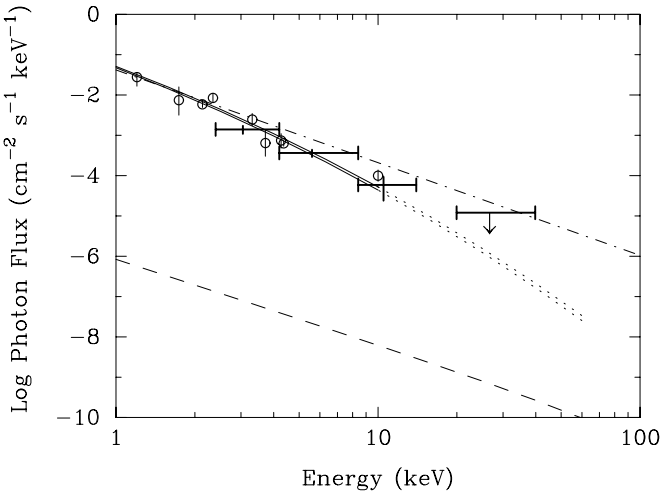

FIG. 2.—Integrated hard X-ray spectrum of SN 1006. The heavy bars show the energy bins over which our JEM-X fluxes are integrated. The integrated fluxes were converted to spectral fluxes assuming a power-law index of 3.0 and plotted at the median energy of each bin. The errors in the bin energies are insignificant (much smaller than the line widths). The upper limit bar is from ISGRI. Open circles are pre-*ASCA* (see text) observations, and the two solid lines are the ± 1 σ model fits to *ASCA* and *RXTE* data, extrapolated to the higher energies (Dyer et al. 2001). The dot-dashed line is the extrapolation from the *Chandra* spectral fit (Long et al. 2003). The dashed line is the bremsstrahlung prediction of the model described in text.

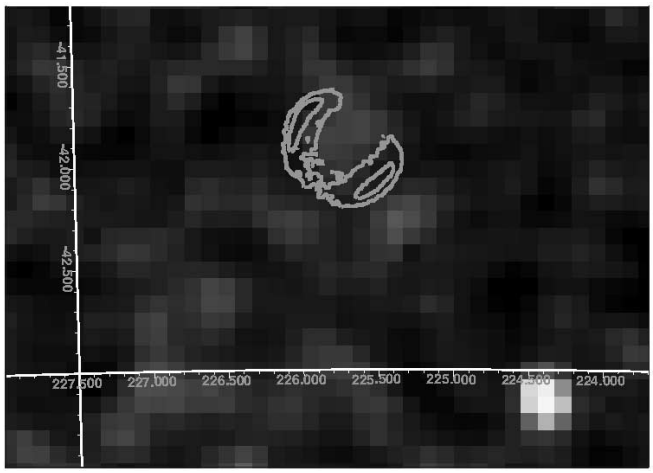

FIG. 3.—ISGRI σ image around SN 1006 in 20–40 keV band. SN 1006 is not detected. A nearby source (possibly VV 780, 11.6 σ detection; Kalemci et al. 2005) is also shown for comparison. The *ASCA* contours are overlaid to show the expected position of SN 1006. The feature at the center of SN 1006 is not significant and is possibly due to inaccurate background map. [*See the electronic edition of the Journal for a color version of this figure.*]

measurements (see Reynolds 1996; Hamilton et al. 1986 for references). The integrated fluxes have been converted to flux densities, assuming a photon index Γ of 3.0 (Allen et al. 2001). Also shown are a pair of model curves for the escape model that provided a good fit to *ASCA* and *RXTE* data in Dyer et al. (2004). The parameters of the best fit are a roll-off frequency of $\nu_{\rm roll} = 3.0 \times 10^{17}$ Hz and an electron energy index of 2.2 (implying a radio spectral index $\alpha = 0.6$ or radio photon index $\Gamma \equiv \alpha + 1 = 1.6$). These parameters imply an *e*-folding energy of the exponential cutoff (due to escape) of $32(B_2/10\ \mu{\rm G})^{-1/2}$ TeV, where B_2 is the postshock field. The curves in Figure 2 correspond to ± 1 σ errors on $\nu_{\rm roll}$, $(2.8{-}3.1) \times 10^{17}$ Hz. The dashed line indicates the bremsstrahlung prediction for an upstream density of 0.2 cm^{-3} and $B_2 = 10$ μG.

3.2. *ISGRI Results*

We obtained ISGRI images in different energy bands using OSA version 4.2. SN 1006 was not detected in any band. The 20–40 keV sigma image is shown in Figure 3. The 3 σ upper limit (sensitivity limit) for a point source for $\sim$750 ks observing time is $\sim 9 \times 10^{-5}$ photons cm^{-2} s^{-1}. If synchrotron radiation dominates in the 20–40 keV band, the emission would be concentrated in two limbs. The extended nature of the source causes a reduction factor of 0.7 in flux (see § 2.2). Therefore, the 3 σ upper limit for a synchrotron-dominated source is 1.3×10^{-4} photons cm^{-2} s^{-1} at each limb. For synchrotron-dominated emission, the expected total flux in the 20–40 keV band (based on the models shown in Fig. 2) is $(2.9{-}3.6) \times 10^{-5}$ photons cm^{-2} s^{-1} for the entire remnant, or roughly half this at each limb. The bremsstrahlung emission from the model shown in Figure 2, using the lower limit 25 μG downstream magnetic field from H.E.S.S. TeV observations, is predicted to be about 2×10^{-8} photons cm^{-2} s^{-1}, far below ISGRI's sensitivity. In fact in this case, since the emission would be coming from a larger area, the upper limit set by our observations is even higher. The predicted crossover energy at which bremsstrahlung and synchrotron emission become comparable is in the vicinity of 200 keV.

Long et al. (2003) reported that a power-law photon index of 2.30 fit the *Chandra* data well between 0.5 and 5 keV for the emission at the limbs. An extrapolation of this fit from 5 keV to the ISGRI range is also shown in Figure 2 with a dot-dashed line. Our ISGRI upper limit is about a factor of 2 below the extrapolation of this power law to 28 keV.

4. DISCUSSION

Coded-mask imaging is a complex process, and optimal techniques are still being developed to clean noisy images, for both JEM-X and ISGRI. Our results confirm and extend results obtained with *ASCA*, *Chandra*, and *XMM-Newton*, and show that relatively small increases in sensitivity may allow ISGRI to detect predicted synchrotron radiation for some models.

The prospect of detecting bremsstrahlung X-rays or gamma-rays from SN 1006 has become considerably more remote with the combination of lower estimates for the ambient density and the much higher magnetic field that would be required to explain the lack of IC from CMB photons in the H.E.S.S. observations. However, it is quite possible that a somewhat longer *INTEGRAL* observation scheduled for Cycle 3 will have sufficient sensitivity to detect synchrotron emission in the 18–40 keV band. A model that can describe the observations of Figure 2 but with a strong enough magnetic field to satisfy the H.E.S.S. constraints (downstream $B > 25$ μG) is somewhat harder than the spectra shown in Figure 2, and predicts a flux in the 18–40 keV band of 0.3×10^{-4} photons cm^{-2} s^{-1}. Some models predict considerably lower fluxes in the 18–40 keV band, so ISGRI detection would not only extend and confirm the presence of hard synchrotron X-rays but could provide useful model discrimination.

We have obtained the first observations with JEM-X of an extended source, between 2.4 and 14 keV. The fluxes we derive are consistent with those of earlier imaging observations where they overlap, and support the identification of the continuum emission of SN 1006 as synchrotron radiation from an electron distribution that is slowly dropping off. Our ISGRI 3 σ upper limit is about a factor of 4 higher than the prediction of the model that best fits the soft X-ray continuum. With ISGRI, we confirm at higher energies than have been previously

reported that the X-ray spectrum of SN 1006 must be steepening. A somewhat longer observation and more developed data analysis techniques should allow the detection of SN 1006 in the 18–40 keV band with ISGRI and above 8.4 keV with JEM-X and can provide important modeling constraints.

E. K. is supported by the European Commission through a FP6 Marie-Curie International Reintegration Grant (INDAM). E. K. acknowledges partial support of TÜBİTAK. E. K. and S. E. B. acknowledge NASA grants NAG5-13142 and NAG5-13093. S. P. R. acknowledges support from NASA grant NAG5-13092.

REFERENCES

Aharonian, F., et al. 2005, A&A, 437, 135
Allen, G. E., Petre, R., & Gotthelf, E. V. 2001, ApJ, 558, 739
Baring, M. G., Ellison, D. C., Reynolds, S. P., Grenier, I. A., & Goret, P. 1999, ApJ, 513, 311
Becker, R. H., Szymkowiak, A. E., Boldt, E. A., Holt, S. S., & Serlemitsos, P. J. 1980, ApJ, 240, L33
Chenevez, J., Lund, N., Westergaard, N. J., Budtz-Joergensen, C., Kretschmar, P., & Walter, R. 2004, in The 5th INTEGRAL Workshop on the INTEGRAL Universe, ed. V. Schönfelder, G. Lichti, & C. Winkler, (Nordwijk: ESA), 837
Dyer, K. K., Reynolds, S. P., & Borkowski, K. J. 2004, ApJ, 600, 752
Dyer, K. K., Reynolds, S. P., Borkowski, K. J., Allen, G. E., & Petre, R. 2001, ApJ, 551, 439
Gaisser, T. K., Protheroe, R. J., & Stanev, T. 1998, ApJ, 492, 219
Goldwurm, A., et al. 2003, A&A, 411, L223
Gros, A., Goldwurm, A., Cadolle-Bel, M., Goldoni, P., Rodriguez, J., Foschini, L., Del Santo, M., & Blay, P. 2003, A&A, 411, L179
Hamilton, A. J. S., Sarazin, C. L., & Szymkowiak, A. E. 1986, ApJ, 300, 698
Kalemci, E., Boggs, S. E., & Lund, N. 2005, Astron. Tel., 410, 1
Koyama, K., Petre, R., Gotthelf, E. V., Hwang, U., Matsuura, M., Ozaki, M., & Holt, S. S. 1995, Nature, 378, 255
Lebrun, F., et al. 2003, A&A, 411, L141
Long, K. S., Reynolds, S. P., Raymond, J. C., Winkler, P. F., Dyer, K. K., & Petre, R. 2003, ApJ, 586, 1162
Lund, N., et al. 2003, A&A, 411, L231
———. 2004, in The 5th INTEGRAL Workshop on the INTEGRAL Universe, ed. V. Schönfelder, G. Lichti, & C. Winkler (Nordwijk: ESA), 723
Pohl, M. 1996, A&A, 307, L57
Renaud, M., Lebrun, F., Terrier, R., Reynolds, S. P., & Kalemci, E. 2006, A&A, submitted
Reynolds, P. S. 1999, Astrophys. Lett. Commun., 38, 425
Reynolds, S. P. 1996, ApJ, 459, L13
———. 1998, ApJ, 493, 375
Reynolds, S. P., & Chevalier, R. A. 1981, ApJ, 245, 912
Rothenflug, R., Ballet, J., Dubner, G., Giacani, E., Decourchelle, A., & Ferrando, P. 2004, A&A, 425, 121
Sturner, S. J., Skibo, J. G., Dermer, C. D., & Mattox, J. R. 1997, ApJ, 490, 619
Tanimori, T., et al. 1998, ApJ, 497, L25
———. 2005, in Proc. of the 29th International Cosmic Ray Conference, Vol. 4, ed. B. Sripathi Acharya et al. (Mumbai: Tata Inst. of Fundamental Research), 215 (http://icrc2005.tifr.res.in/htm/conf_proceedings.htm)
Ubertini, P., et al. 2003, A&A, 411, L131
Vedrenne, G., et al. 2003, A&A, 411, L63
Winkler, P. F., & Laird, F. N. 1976, ApJ, 204, L111
Winkler, C., et al. 2003, A&A, 411, L1